ISGSR2007 First International Symposium on Geotechnical Safety & Risk
Oct. 18~19, 2007 Shanghai
Tongji University, China

Experimental Study of the Light Dynamic Penetration Method to Test Shallow Fill of Coarse-sand in Subsoil Engineering

TIAN Qingyan, Fu Helin
Civil Engineering College of Central South University, Changsha Hunan,
Guangdong Transportation and Communication Testing Center, Guangdong Guangzhou, China

ABSTRACT: In this paper, experimental relationship between light dynamic penetration blow counts N_{10} and relative density Dr of coarse-sand is built on the base of large model tests by simple statistics. Then, the feasibility of this mothed is proved by three-dimension numerical calculation and field tests. It shows that the light dynamic penetration can be well applied in testing the density of coarse sand at shallow coarse-sand back filling subground.

1 INTRODUCTION

Light dynamic penetrating test is a common method of in-situ test. It utilizes certain hammer force to hit the drill pile into soil and to evaluate the soil properties according to the penetrating force, which, under certain conditions, reflects the differences of mechanics property of soil layer. Because the light dynamic penetrating apparatus is handy, portable and convenient to handle, many researches in the world have launched in this field and gained much achievement ever since the 1950s. Meanwhile, the application of the light dynamic penetrating test method in the sand soil has been improved greatly. However, due to the weak hitting force and the easy bending of the pile, this method used to be considered applicable only in differentiating the soil bed and in evaluating the isotropy of the layers in fine sand soil. At present, its application in testing the relative density of coarse-sand backfill has not been studied systematically.

In this paper, in order to carry out the application of the light dynamic penetrating test in testing the relative density of coarse-sand backfill, four kinds of sand in different grain sizes and different densities are used to proceed a series of light penetrating tests in the model trough and to disclose the experimental relationship between light dynamic penetration blow counts (N_{10}) and relative density (Dr) of coarse-sand. The relationship is also simulated by the three-dimensional finite numerical analysis, by the consistency between the soil stress obtained in the test and the result obtained in 3-D FEM analysis, this paper vertifies the reliability of the relative density of coarse sand in the light dynamic penetrating test. Otherwise, the experimental relationship between the light dynamic penetration blow counts (N_{10}) and relative density (Dr) is valid by field test.

2 RESULTS OF THE LARGE MODEL TEST

In this study, four kinds of typical sand (Table 1 and Fig. 1) are chosen in back sand filling of subsoil, and the model test is proceeded in a model sink (2m×2m×2m) to collect index, such as relative density Dr, the light dynamic penetration blow counts N_{10}, stress of sand at different depth in model test, analyze the feasibility that the light dynamic penetration is used to test the density of coarse sand at shallow coarse-sand back filling in Subsoil Engineering, and build the experimental relationship between blow counts N_{10} and relative density Dr. Results of test are shown in Tables 2-5.

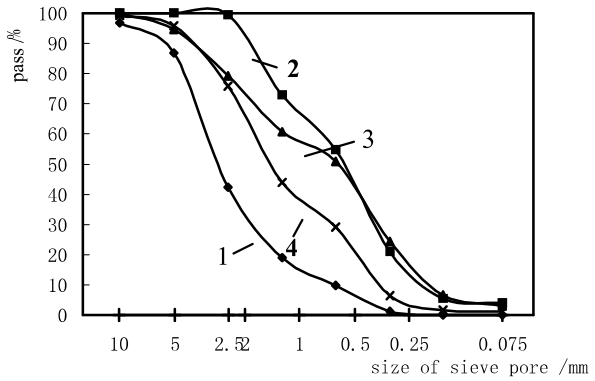

1, sand No. 1; 2, sand No. 2; 3, sand No. 3; 4, sand No. 4

Fig. 1 Composition of sand in model test

2.1 Critical depth (h_{cr})

The surface layer of sand should not be neglected to detect relative density of sand by light dynamic penetration. But because it is affected by the effect of surface layer and the dead weight of sand, the light dynamic pentration blow count N_{10} is increasing gradually with the further depth of pentration ing certain range of the surface depth. The paper plans to gain the regularity that the blow counts change with depth in the range of penetration in order to control the countruction quality of coarse-sand back filling reasonably and evaluate the relative density effectively. So it is necessary to determine the critical depth of light dynamic penetration and research into the regularity that the blow counts change with depth above or below the critical depth.

From Figs. 2-5, it shows that light dynamic penetration blow count N_{10} increases with the further penetration, and when the cone explore into a certain depth, it reaches the maximum which is called critical depth (h_{cr}). The curves of h_{cr} and Dr of the four kinds sand as showed in Fig. 6 reveal that h_{cr} exists in reality and it increases nonlinearly with Dr.

Table 1 Physical index of the testing sand

Serial number of Sand	Fineness M_X	G_s	e_{max}	e_{min}	F	d_{50}(mm)	C_u	C_c	Class[1]
No. 1	4.17	2.65	0.941 0	0.386 2	1.435 8	2.85	5.54	1.76	Gravel
No. 2	2.47	2.63	1.029 3	0.461 1	1.232 3	0.56	3.49	0.90	Near fine sand
No. 3	2.66	2.65	0.798 0	0.409 6	0.947 8	0.60	6.18	0.61	Mesne sand
No. 4	3.36	2.66	0.971 0	0.440 9	1.201 4	1.45	5.00	0.59	Coarse sand

Note: $F=(e_{max}-e_{min})/e_{min}$; The mineral composition of sand is quartz.

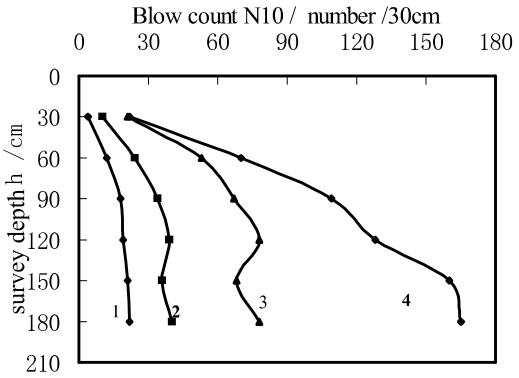

1, Dr=0.54; 2, Dr=0.70;
3, Dr=0.81; 4, Dr=0.89

Fig. 2 Results of No.1 sand

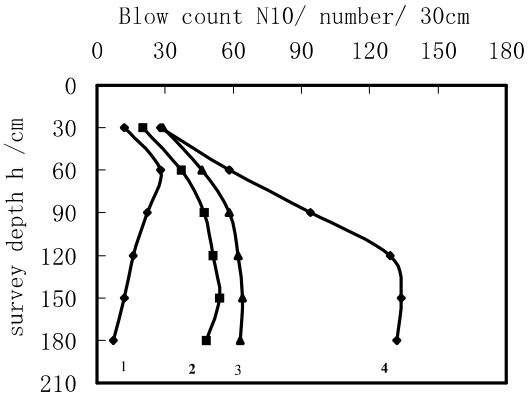

1, Dr=0.49; 2, Dr=0.66;
3, Dr=0.73; 4, Dr=0.93

Fig. 3 Results of No.2 sand

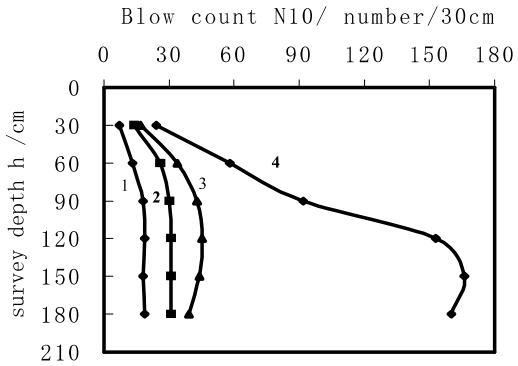

1, Dr=0.49; 2, Dr=0.59;
3, Dr=0.74; 4, Dr=0.90;

Fig.4 Results of No.3 sand

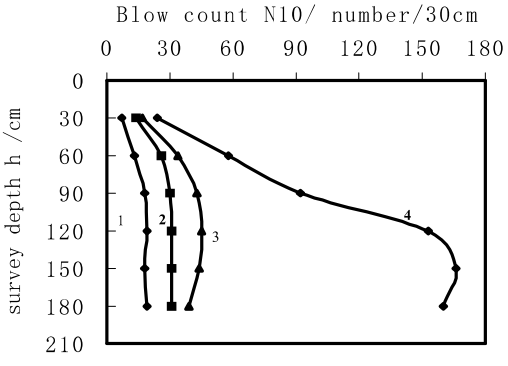

1, Dr=0.49; 2, Dr=0.62;
3, Dr=0.76; 4, Dr=0.93;

Fig.5 Results of No.4 sand

2.2 Blow count (N_{10}) of light dynamic Petrenation

According to the results of model tests if bigger than the criticle depth, N_{10} of light dynamic petrenation increases with the petrenating depth (h) and relative density of sand (Dr); if smaller than the critical depth h_{cr}, N_{10} stays stable. As the test result showed, Dr is the most sensitive factor to influence the blow count N_{10L} in the critical depth, it can be concluded that the blow count N_{10L} in the critical depth increase considerably with the increase of Dr.

In addition, there exists a bridge between the blow count N_{10L} and the fineness modulus Mx of sand. When Dr＜0.80 but N_{10L} is fixed, the larger the fine modulus Mx is, the larger the relative density is, the order of Dr is as followings: gravel, coarseness, intermediate, and fineness.

2.3 Experiential formula of Dr and N_{10} from model test

On the base of the features of petrenating curve, the analysis of the relationship between N_{10} and Dr may be divided into two kinds of conditions by considering the critical depth as a boundary.

Above the critical depth (h_{cr}), according to *Kreim Theorem*, there exists pluralistic and linear relationship between relative density of sand (Dr) and fineness modulus of sand (Mx), exploration depth (h), blow count (N_{10}, the number of blow counts per 30cm), as showed in formula (1); at the critical depth and its below, Dr is in logarithm with N_{10L} through nonlinear analysis, as showed in formula (2).

$$D_r=0.3237+0.1090M_x-0.0037h+0.007N_{10} \quad (\rho=0.9175). \tag{1}$$

$$D_r=-0.1057+0.2080\ln(N_{10L}) \quad (\rho=0.9368) \tag{2}$$

In the above formula, Dr---- the relitive density of sand, N_{10} ---- the blowcount of light dynamic penetration above the critical depth, Mx ---- the fineness modulus of sand, h ---- the exploration depth of light dynamic penetration, N_{10L} --- the blow counts of light dynamic penetration at the critical depth.

As concluded in formula 1, above critical depth, except N_{10}, the fineness modulus of sand influences Dr is to the most. When other parameters are fixed, the larger Mx is, the bigger the relative density of sand will be.

3 CALCULATION ON THREE-DIMENSION- FINITE UNITS

Aided by the three-dimensional finite elements, the testing results of the light dynamic petrenation are further examined. Simultaneously, the stress, strain, the features of displacement distribution and distribution curve diagram of sand in the process of dynamic exploration are calculated in sand of different relative density. In the model procedure, the p. V. lade model is adopted, parameter units such as the ten-cross-point tetrahedron are used, as shown in Fig. 7.

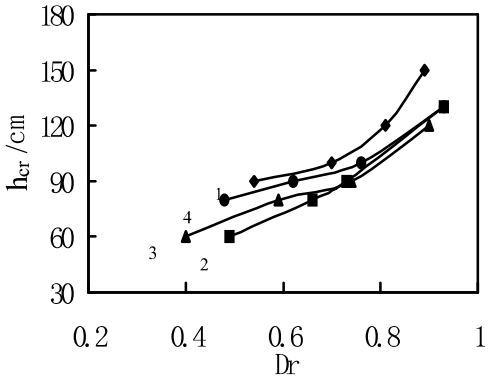

1, sand No. 1; 2, sand No. 2; 3, sand No. 3; 4, sand No. 4

Fig. 6 Test relation between h_{cr} and D_r

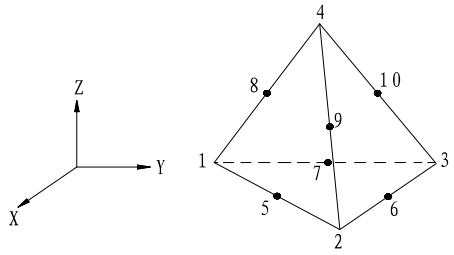

Fig.7 The unit cross-points in the whole coordinate system

For partial coordinate, function insertion by adopting cross-point displacement amount can be directly obtained from the unit displacement function.

$$\begin{cases} u=\sum_{i=1}^{m}N_i(\xi,\eta,\zeta)u_i \\ v=\sum_{i=1}^{m}N_i(\xi,\eta,\zeta)v_i \\ w=\sum_{i=1}^{m}N_i(\xi,\eta,\zeta)w_i \end{cases} \tag{3}$$

In the above formula, u, v, w represents the displacement of unit along x, y and z reference axis respectively, $N_i(\xi,\eta,\zeta)$ is shape functio, ξ,η,ζ is cross-point coordinate in part of reference frame, u_i, v_i, w_i represent the displacement of the cross-point i.

The often-used mother unit of the parameter units such as the usual tetrahedron includes the four cross-point linear tetrahedron unit and the ten cross-point quadratic tetrahedron unit etc. (shown in fig.5). The shape functions is:

$$N_i=(2L_i-1)L_i. \tag{4}$$

here, $i=1$，2，3，4； L_i is the ratio of a sub-tetrahedron volume formed by a random point and one side in tetrahedron and that of the tetrahedrom.

To the cross-point in amidst side：

$$\begin{cases} N_5 = 4L_1L_2 \\ N_6 = 4L_2L_3 \\ N_7 = 4L_1L_3 \\ N_8 = 4L_4L_1 \\ N_9 = 4L_2L_4 \\ N_{10} = 4L_3L_4 \end{cases} . \tag{5}$$

By deduction, the unit's stiffness matrix $\mathbf{K}^e$ is expressed as the following equation：

$$\mathbf{K}^e = \int_{\Omega_e} \mathbf{B}^T \mathbf{D} \mathbf{B} t dA = \int_0^1 \int_0^{1-\xi} \int_0^{1-\xi-\eta} \mathbf{B}^T \mathbf{D} \mathbf{B} |\mathbf{J}| t d\xi d\eta d\zeta . \tag{6}$$

where：B stands for strain matrix of the unit, t is thickness; $\mathbf{J}$ is three-dimensional Jacobi matrix; $\mathbf{D}$ is elastic matrix.

The general stiffness matrix can be formed according to formula(6), then the displacement direction $\{\boldsymbol{\delta}\}$ of a unit can be obtained by the borderary condition and its loading $\{\mathrm{R}\}$.

$$[\mathbf{K}]\{\boldsymbol{\delta}\} = \{\mathrm{R}\} . \tag{7}$$

Then, the unit stress and strain can be concluded, based on the equation $\{\boldsymbol{\varepsilon}\}=[\mathbf{B}]\{\boldsymbol{\delta}\}$ and $\{\boldsymbol{\sigma}\}=[\mathbf{D}]\{\boldsymbol{\varepsilon}\}$.

In the nonlinear FEM analysis, the combination of the elastic modulus matrix, which is needed in the increment calculation, is the key problem.

As the Lade model has two yield surfaces, the elastic-plastic modulus matrix has the following forms:

$$[\mathbf{D}]_{ep} = [\mathbf{D}] - \frac{G[\mathbf{X}]}{B_1 B_2 - \Phi_{f_1 g_1} \Phi_{f_2 g_2}} . \tag{8}$$

In the formula: $B_1 = \frac{A_1}{G} + \Phi_{f_1 g_1}$； $B_2 = \frac{A_2}{G} + \Phi_{f_2 g_2}$； $[\mathbf{X}] = B_2[\mathbf{X}_{f_1 g_1}] + B_1[\mathbf{X}_{f_2 g_2}] - \Phi_{f_1 g_1}[\mathbf{X}_{f_2 g_1}] - \Phi_{f_2 g_2}[\mathbf{X}_{f_1 g_2}]$

f_1 、f_2 represent yield functions of the first and the second yield face of the Lade model hyperboloid; g_1，g_2 stand for plastic potential functions of the first and the second yield face.

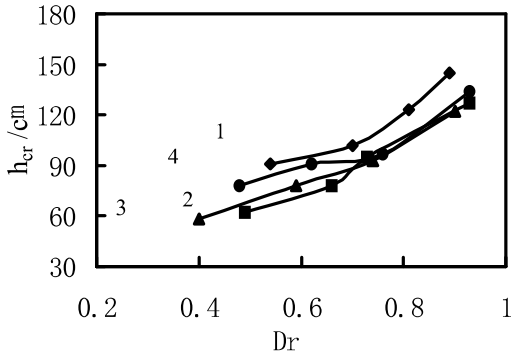

1, sand No. 1; 2, sand No. 2; 3, sand No. 3; 4, sand No. 4

Fig. 8 Calculation relation between h_{cr} and D_r

3.1 Comparison of critical depth by calculation and model test

By computing, the relationship between critical depth and relative density is shown in Fig. 8. As shown in Fig. 6 and Fig. 8, for critical depth, the result by calculation is quite close to the result in the model test. When the relative density is between 0.40 and 0.80, the sixe order of critical depth h_{cr} is as followings: sand No. 1, sand No.4, sand No. 3 and sand No.2.

3.2 Analysis about calculational and testing stress and strain

The testing soil stress and strain during petrenating process are obtained from four soil stress boxes No.10, No.11, No.12, No.13, which are filled respectively in soil with depth of 45cm, 115cm, 76cm and 155cm. During the process of penetration, the maximum stress and strain in sand take place in the place where is a little bit above the soil stress box. The shape os close to an ellipse. In Fig. 10 and Fig. 11, the comparison between the stress and strain curve gained by finite element method and the same type of curve gained by test in the soil stress box is shown. It is clear that the calculation value is close to the test value.

Through finite element calculation, it is known that, ever since the beginning of the drill head penetrating into the sand surface, soil around the drill head in sand of relatively great density has the tendency of flow upward, and apparent upheaval and crack can be seen on the surface.

When the penetrating reaches certain depth and the depth is within the critical depth, the former stress in some parts of the two sides of the drill head lax or diminishes, (the testing subordinate stress should be a negative value, shown in Figs. 9-10). This belongs to typical failure mechanism. While sand in small relatively density is mainly controlled by the compress and penetrating mechanism, its surface has no apophysis or unconspicuous apophysis in drilling. Due to the differences of the penetrating mechanism in different relative densities and different scopes, there exists obvious differences in the stress, strain and displacement in sand of different densities. when the penetration beyond the critical depth, the critical stress(σ_3)of the sand of relative small density which is controlled by the contracting mechanism is weak, and the scope the mechanism works is not wide, the cover press of soil almost doesn't work. However, for the sand of relative great density over the critical depth, its critical stress is strong and its soil press influence is also great. Therefore, the stress value in the critical depth h_{cr} is bigger than that of small density.

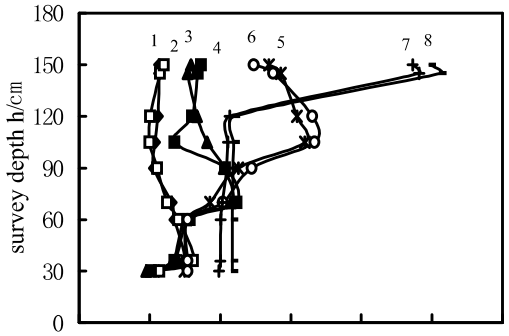

1, Test stress of soil stress box 10 in No. 1 bore
2, Cal. stress of soil stress box 10 in No. 1 bore
3, Test stress of soil stress box 12 in No. 2 bore
4, Cal. stress of soil stress box 12 in No. 2 bore
5, Test stress of soil stress box 11 in No. 3 bore
6, Cal. stress of soil stress box 11 in No. 3 bore
7, Test stress of soil stress box 13 in No. 4 bore
8, Cal. stress of soil stress box 13 in No. 4 bore

Fig.9 Comparison of calculation and test stress of sand No. 4

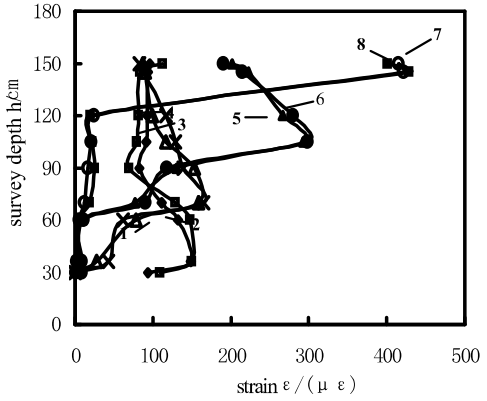

3, Test strain of soil stress box 12 in No. 2 bore
4, Cal. strain of soil stress box 12 in No. 2 bore
5, Test strain of soil stress box 11 in No. 3 bore
6, Cal. strain of soil stress box 11 in No. 3 bore
7, Test strain of soil stress box 13 in No. 4 bore
8, Cal. strain of soil stress box 13 in No. 4 bore

Fig.10 Comparison of calculation and test strain of sand No. 4

In order to verify the feasibility of the application of the results of light dynamic penetration model test, field tests are carried out in constructing roadbed engineering adopting same apparatus and

similar sand with fineness modulus of 3.00. Three groups of test datum of filling sand in a culvert-back are shown in Fig. 11.

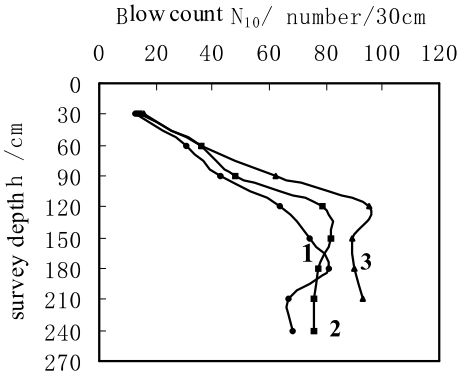

1, point1#-3； 2, piont0#-1； 3, point 0#-2

Fig.11 Relation between N_{10} and h of light dynamic petrenating

Contrast of Fig. 11 with Figs. 2-5, the curve form in field test is consistent with that of model test. Table 2 lists the testing density of sand in deferent depth and its corresponding calculational value, which is gained by inserting blow counts (N_{10}) data of field test No. 1#-3 into formula (1) and (2). From table 6, error or relative error between calculational and testing Dr of field sand is less than 10 percent can be acquired. So it proves that it is feasible and valid for the formula (1) and (2) to be applied to light dynamic petrenation testing relative density of shallow fill coarse-sand subground.

Table 2 Comparison between Dr calculated and Dr tested of No. $1^{\#}$-3 coarse sand on the spot

M_X	h	N_{10}	Calculational value	Test value	Difference/Ratio	Remark
3.00	30	28	0.73	0.76	-0.03/-3.9%	
3.00	60	44	0.73	0.76	-0.03/-3.9%	
3.00	90	59	0.72	0.76	-0.04/-5.3%	
3.00	120	80	0.81	0.76	0.05/6.6%	The critical depth in the field test
3.00	150	75	0.79	0.76	0.03/3.9%	

5 CONCLUSIONS

From above, four points can be concluded as followings:

(1) During the light dynamic petrenation testing, Dr of sand is the most sensitive factor to the blow counts (N_{10}), and the fineness modulus of sand is the next one.

(2) By analyzing model test data, above the critical depth (h_{cr}) of sand layer, there exists linear relationship between the relative density of sand (Dr) and N_{10}. By adopting Kreim principle, it is regressed to get formula (1); at critical depth and below it, the connection between N_{10L} and Dr can statisfy a logarithm function, and it is regressed to get formula (2).

(3) Simulated by the three-dimensional FEM, the calculational stress and strain in soil is consistent with that of testing value, which confirms it verified in theory that it is feasible for light dynamic petrenation detecting the relative density of back-fill coarse sand in subground works.

(4) By field test, it is clear that the relative density of sand gained by adopting experiential formula (1) (2) is consistent with the test value of it. So formula (1) (2) from model test may by applied to calculate the relative density of carse sand.

ACKNOWLEDGMENTS.

This paper is a part of the project report of *Testing Method Study of the Relative Density of Back*

Filling Coarse Sand in Transition of Bridge and Roadbed in Highway Construction (No. 2002-13) sponsored by the Science and Technology Foundation of Guangdong Transportation Governmemt.

REFERENCES

Chang Aiguo, Du Ronghua, Fan Pengfei. 'The Application of PANDA Dynamic Penetration Device to Highway', Shanxi Science & Technology of Communications, 2001, 144(2): 53-55

Code for Investigation of Geotechnical Engineering, GB50021-2001, PRC Standard, 2002.

De Beer, E E. Donness concarnant la resistance an oisaikllement decluities des en ais de penetration en profondeur. Geotechnique, 1948, 1(1): 22-40.

Deng bo,The Statistic Method of Analyzing test data, Tsinghua University Press, Beijing, 1997. P248～256.

Durgunoglu H T, Mitchell J K. Static penetration resistance of soils I: Analysis. In: Raleigh N C,ed. Proc ASCE Spec Conf on In Situ Measurement of Soil Properties, New York, ASCE, 1975-01-06-10. 151-171.

Hu G.Bearing capacity of foundations with overburden shear. Sols-Soils, 1965, 2(13): 11～18
Lu Zhaohui,. "Dynamic Penetration Test on a Bridge Base", Journal of Anhui University of Science and Technology(Natural Science), 2003, 23(2) : 14～17.

Mahmoud, M, Woeller D,Robertson P K. Detection of shear zones in a natural clay slope using the cone penetration test and continuous dynamic sampling. Canadion Geotechnical Journal, 2000, 37(3): 652-661.

Pankin,A.K., Lunne, T., Boundary Effects in the laboratory Calibration of a cone penetration for sand, ESOPT-Ⅱ, 1982.

Robertson P K, Campanella R G. Interpretation of cone penetration tests Part 2: clay. Can Geotech J, 1983, 20(4): 734-745.

Tang Xianqiang, In-situ Test Technology in Foundation Project. Beijing: China Railway Press, 1996.

Terzaghi K. Theoretical soil mechanics. New York: John Wiley & Sons, 1943.

The FEM simulation of dynamic penetration process of CPTU.Ma Shu-Zhi,etc, Rock and soil mechanics 2002, 23(4): 478-481.

Xie Shouyi, Xu Weiya, Liu Defu, Jiang Ping. 'A General Index of Dynamic Penetration Test–Dynamic Cone Resistance and Its Application', Journal of University of Hydraulic and Electric (Yichang), 1998, 20(3): 39-42.

Yu H S, Mitchell J K Analysis of cone resistance: review of methods. Journal of Geotechnical and Geoenvironmental Engineering, ASCE, 1998, 124(2): 140～149